Journal of Magnetism and Magnetic Materials 383 (2015) 250–254

Contents lists available at ScienceDirect

Journal of Magnetism and Magnetic Materials

journal homepage: www.elsevier.com/locate/jmmm

# Spectral signatures of spin–phonon and electron–phonon interactions in multiferroic iron borates

M.N. Popova [a,*], K.N. Boldyrev [a], S.A. Klimin [a], T.N. Stanislavchuk [b], A.A. Sirenko [b], L.N. Bezmaternykh [c]

[a] Institute of Spectroscopy, RAS, Moscow, Troitsk 142190, Russia
[b] Department of Physics, New Jersey Institute of Technology, Newark, NJ 07102, USA
[c] Kirenskiy Institute of Physics, Siberian Branch of RAS, Krasnoyarsk 660036, Russia

ARTICLE INFO

*Article history:*
Received 24 June 2014
Received in revised form
18 October 2014
Accepted 20 October 2014
Available online 23 October 2014

*Keywords:*
Rare-earth iron borates
Spin–phonon interactions
Electron–phonon coupling
Optical spectroscopy

ABSTRACT

High-resolution far-infrared reflection and polarized ellipsometry, as well as Raman scattering temperature-dependent measurements are used to study spin-phonon and electron-phonon interactions in rare-earth (RE) iron borates with the R32 structure of a natural mineral huntite, namely, in $RFe_3(BO_3)_4$ with R=Pr, Nd, and Sm. Pronounced peculiarities in the $\omega(T)$ dependences at the Néel temperature $T_N \approx 32$ K are observed for all the compounds studied and the origin of these peculiarities is discussed. A coupling between lattice phonons and crystal-field excitations of a RE ion manifests itself by a renormalization of frequencies and intensities of coupled modes. Modeling of the spectra has revealed the value of about 15 $cm^{-1}$ for the electron–phonon coupling constant in $PrFe_3(BO_3)_4$.



## 1. Introduction

Charge–lattice–spin coupling plays a key role in a vast variety of phases and phenomena observed in multiferroics [1–3]. To study these interactions, different methods are used, in particular, optical ones. Thus, pronounced phonon anomalies around the Néel temperature $T_N$ were observed in the Raman spectra of multiferroic $BiFeO_3$ [4] and $RCrO_3$ (R stands for a rare earth or yttrium) [5] and in the far infrared (FIR) spectra of $EuFe_3(BO_3)_4$ [6]. Anticrossing between the magnetic exchange excitation and the $Tb^{3+}$ crystal-field (CF) excitation in the FIR spectra of a multiferroic garnet $Tb_3Fe_5O_{12}$ and a formation of hybrid *f*-electron–magnon excitations were recently demonstrated in Ref. [7].

The present paper deals with FIR and Raman studies of spin–phonon and electron–phonon interactions in rare-earth (RE) iron borates $RFe_3(BO_3)_4$ that belong to an interesting new family of multiferroics. These compounds crystallize in a huntite-type noncentrosymmetric trigonal structure characterized by a presence of helical chains of edge-sharing $FeO_6$ octahedra running along the *c*-axis of the crystal, interconnected by two kinds of $BO_3$ triangles and $RO_6$ distorted prisms [8], see Fig. 1. In the case of R=Pr, Nd, and Sm, the structure is described by the space group R32 at all the temperatures. Just this subfamily is studied in the present work. As for the rest $RFe_3(BO_3)_4$ compounds, they undergo a structural phase transition $R32$–$P3_121$ with lowering the temperature [9,10]. A presence of two interacting magnetic systems (RE and iron ones) results in a large diversity of RE dependent magnetic and magnetoelectric properties of iron borates. All of them order magnetically at temperatures 30–40 K [11] but into different, sometimes complicated, magnetic structures depending on the R ions. Of the compounds studied here, $NdFe_3(BO_3)_4$ ($T_N$ =33 K) [12–14] and $SmFe_3(BO_3)_4$ ($T_N$=32 ± 1 K) [15–17] order into the easy-plane antiferromagnetic structure while $PrFe_3(BO_3)_4$ ($T_N$ =32 ± 1 K) [18–21] orders into the easy-axis one. At 13.5 K [13] (16 K [14]) a commensurate magnetic structure of $NdFe_3(BO_3)_4$ turns into an incommensurate spin helix that propagates along the *c* axis [13,14]. Large magnetoelectric and magnetodielectric effects were registered in the neodymium and samarium iron borates [22–25].

## 2. Experiment

$PrFe_3(BO_3)_4$, $NdFe_3(BO_3)_4$, and $SmFe_3(BO_3)_4$ single crystals of good optical quality were grown in the Kirenskiy Institute of Physics in Krasnoyarsk, as described in Ref. [19]. Samples with dimensions up to $5 \times 5 \times 10\ mm^3$ were oriented using the crystal morphology and optical polarization methods. A Fourier

* Corresponding author.
*E-mail address:* popova@isan.troitsk.ru (M.N. Popova).

http://dx.doi.org/10.1016/j.jmmm.2014.10.095
0304-8853/

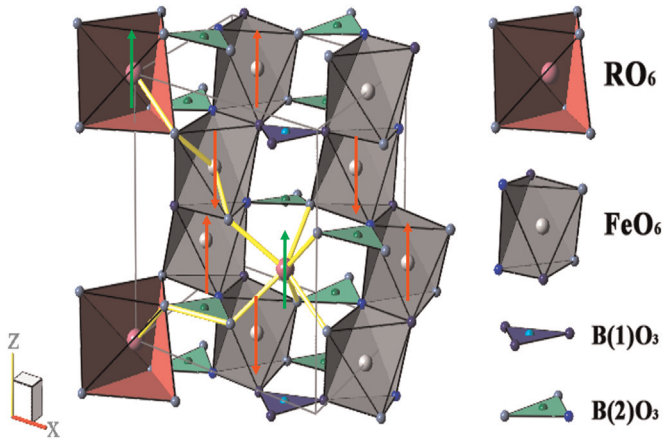


**Fig. 1.** A fragment of the crystal structure of $RFe_3(BO_3)_4$. Each $R^{3+}$ ion is connected by R–O–Fe bonds to six $Fe^{3+}$ ions residing in the three chains of $FeO_6$ octahedra (only two of them are shown) around this $R^{3+}$ ion. These $Fe^{3+}$ ions are situated in the (001) and (00−1) planes above and below the $R^{3+}$ ion, which supports a nonfrustrated magnetic interaction between the $R^{3+}$ ion and antiferromagnetically ordered iron chains below $T_N$. Red and green arrows indicate directions of magnetic moments for $Fe^{3+}$ and $Pr^{3+}$ ions in the magnetically ordered state of $PrFe_3(BO_3)_4$ where Fe–Pr interaction is antiferromagnetic [20,21]. (For interpretation of the references to color in this figure legend, the reader is referred to the web version of this article.)

spectrometer Bruker IFS 125 HR with a liquid helium bolometer (4.2 K) as a detector and a closed helium cycle cryostat Cryomech ST403 were used to register optical reflectance spectra in the spectral region 0.6–3 THz (20–100 $cm^{-1}$) in the $\pi$-($\mathbf{k}\perp c$, $\mathbf{E}\parallel c$, $\mathbf{H}\perp c$) and $\sigma$- ($\mathbf{k}\perp c$, $\mathbf{E}\perp c$, $\mathbf{H}\parallel c$) polarizations, in a broad range of temperatures (3–300 K). FIR ellipsometry measurements were also performed, using a self-made ellipsometer on the U4IR beamline of the National Synchrotron Light Source, Brookhaven National Laboratory, USA [26]. Raman measurements were performed in a backscattering configuration, as described in Ref. [10].

## 3. Results and discussion

As we intend to study interactions between lattice vibrational excitations and the spin and electronic subsystems of $RFe_3(BO_3)_4$, R=Pr, Nd, Sm, that belong to the $R32$ ($D_7^3$) space symmetry group, we have to remind what phonons can be probed in them by optical measurements. These compounds have one formula unit in a primitive crystal cell (20 atoms), so their vibrational spectrum consists of 60 branches. 57 optical $\Gamma$ point ($k=0$) phonons are characterized by irreducible representations of the crystal factor group $D_3$ as follows [10]: $\Gamma_{vibr}=7\ A_1(xx,yy,zz)+12\ A_2(E\parallel z)+19\ E\ (E\perp z,\ xy,xz,yz)$. The $A_2$ ($E$) phonon modes are IR active for the electric vector of radiation polarized along (perpendicular to) the $c$ crystalline axis. $E$ modes are also Raman active, as well as $A_1$ modes. Recently, the data on the IR active phonons in Pr, Nd, and Sm iron borates at room temperature (RT) were published [27]. The RT Raman data on $NdFe_3(BO_3)_4$ are presented in Ref. [10].

### 3.1. Spectral manifestations of a spin–phonon coupling in RE iron borates

Fig. 2 displays the temperature dependences of some phonon frequencies in $NdFe_3(BO_3)_4$ and $PrFe_3(BO_3)_4$. Pronounced peculiarities are observed at the temperature $T_N$ of the antiferromagnetic ordering. Two mechanisms, the static one and the dynamic one, of a coupling between lattice phonons and a magnetic ordering of the system have to be considered. The static mechanism originates from the magnetoelastic coupling in a multiferroic material. In a magnetically ordered state, internal local magnetic fields give rise to static atomic displacements (some kind of a local magnetic striction) which may change interatomic distances and elastic constants and thus influence the phonon frequencies. The dynamic mechanism of spin–phonon coupling is based on the phonon-induced modulation of the superexchange energies, which, in its turn, affects the elastic constants and, hence, the phonon frequencies [28]. In Ref. [6], an experimental evidence was presented for static atomic displacements in a magnetically ordered state of $EuFe_3(BO_3)_4$. Probably, such displacements exist in a magnetically ordered state of other RE iron borates. In Ref. [6], however, it was not possible to determine a quantitative contribution of this mechanism into observed shifts of $EuFe_3(BO_3)_4$ phonon frequencies at $T_N$.

As for the dynamic mechanism, in the case of a nonresonant spin–phonon interaction the temperature dependence of the phonon frequency reads [29]:

$$\omega_n^2(T) = \omega_{n0}^2 + \sum_{ij} C_{ij}^n \langle S_i S_j \rangle (T) \quad (1)$$

Here, spin products in the Heisenberg Hamiltonian are approximated by their temperature-dependent effective averages; $C_{ij}^n$ coefficients are characteristics of the spin–phonon interaction. In principle, $C_{ij}^n$ may have any sign, depending on the eigenvector of a particular phonon mode, which explains why both hardening and softening of phonon frequencies upon magnetic ordering are observed. To get quantitative information on the spin–phonon interaction in iron borates, a microscopic theory has to be developed.

Besides noticeable peculiarities at $T_N$ in the phonon frequencies vs temperature dependences for $RFe_3(BO_3)_4$ compounds, Fig. 2 demonstrates also a substantially different and $R^{3+}$ ion dependent behavior of phonon frequencies above $T_N$. An interaction between lattice vibrations and electronic crystal-field excitations of $R^{3+}$ ions could be the most probable reason for that. We begin the next Section with comparing $\omega(T)$ curves for the lowest-frequency $E$ phonon in $PrFe_3(BO_3)_4$ [Fig. 2(b)] and $NdFe_3(BO_3)_4$ [Fig. 2(a)].

### 3.2. Interaction between lattice phonons and crystal-field levels of $R^{3+}$ ions in $RFe_3(BO_3)_4$

Fig. 2 evidences a drastic difference in the temperature behavior of the lowest-frequency in-plane lattice vibration of $PrFe_3(BO_3)_4$ and $NdFe_3(BO_3)_4$. In $PrFe_3(BO_3)_4$, this vibration markedly softens upon lowering the temperature, whereas in $NdFe_3(BO_3)_4$ it strongly hardens. The lowest-frequency CF excitation of the $\Gamma_3$ symmetry (which is allowed to interact with $E$ phonons) lies at 192 $cm^{-1}$ for $PrFe_3(BO_3)_4$ [20], i.e., above the 85 $cm^{-1}$ phonon mode, and at 65 $cm^{-1}$ for $NdFe_3(BO_3)_4$ [30], i.e., below the considered mode. A mutual "repulsion" of the interacting excitations results in such a different behavior of the lowest-frequency $E$ phonon in the praseodymium and neodymium compounds. A further support of such interpretation comes from the temperature-dependent FIR ellipsometry data on $NdFe_3(BO_3)_4$ [Fig. 3]. An interaction between the $E$ phonon mode and the electronic excitation of the $\Gamma_3$ ($E$ in phonon notations) symmetry (corresponding to the $\Gamma_4$–$\Gamma_{56}$ transition between the $Nd^{3+}$ CF levels) is observed. The quasielectronic mode gains its intensity at the expense of the $E$ phonon mode which looses its intensity with lowering the temperature.

The most spectacular manifestations of the electron–phonon coupling are observed in the FIR spectra of $PrFe_3(BO_3)_4$. Fig. 4 presents the $\pi$-polarized FIR reflection spectra due to $A_2$ non-degenerate phonon modes and the corresponding reflection intensity maps for $PrFe_3(BO_3)_4$ and, for a comparison, $SmFe_3(BO_3)_4$.

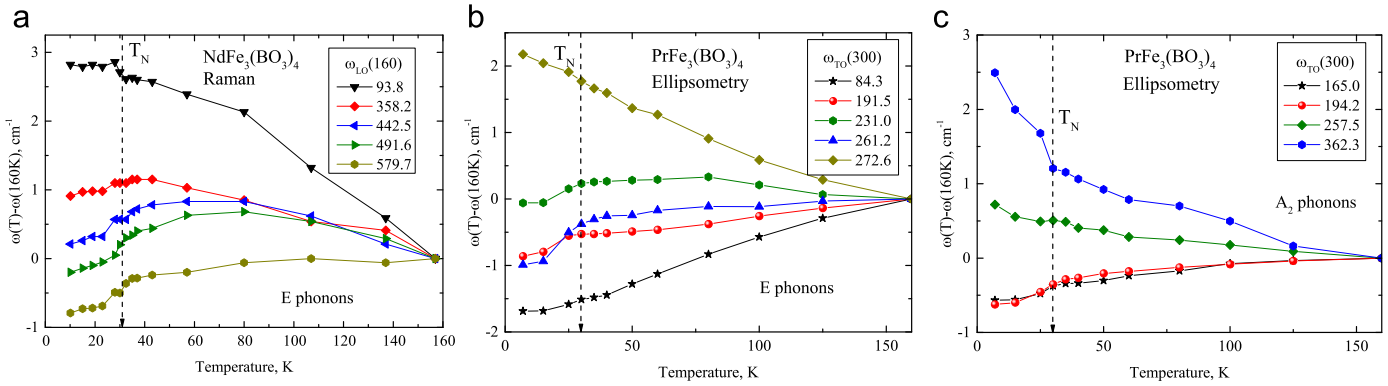


**Fig. 2.** Temperature dependences of phonon lines' positions in (a) $NdFe_3(BO_3)_4$ and (b and c) $PrFe_3(BO_3)_4$. (a) Raman and (b and c) FIR ellipsometry data are presented.

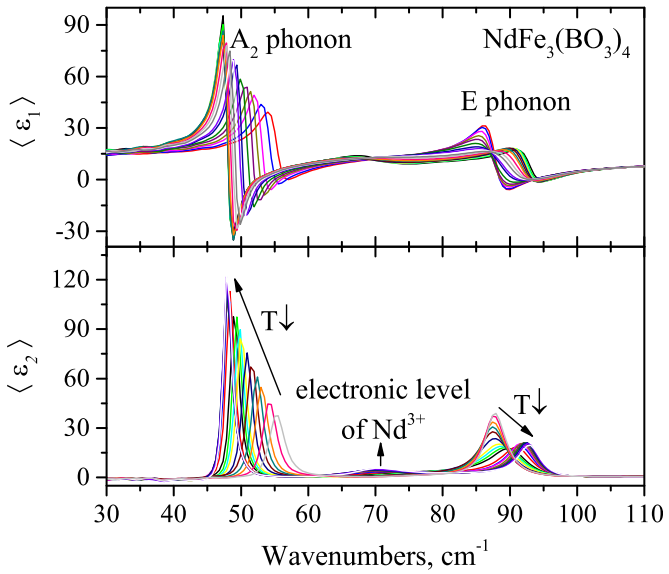


**Fig. 3.** The real $<\varepsilon_1(\omega)>$ and imaginary $<\varepsilon_2(\omega)>$ parts of the pseudo-dielectric function of $NdFe_3(BO_3)_4$ obtained from the ellipsometry data at different temperatures.

In the spectra of the Sm compound, only a small kink at $T_N$ in the $\omega(T)$ dependence for the $A_2^2$ phonon mode is observed, whereas the lowest-frequency $A_2^1$ mode does not change at all with lowering the temperature. By contrast, for $PrFe_3(BO_3)_4$ a splitting of the reststrahlen (reflection) band corresponding to the $A_2^1$ mode is clearly seen. The splitting starts below ~100 K, well above $T_N$ =32 K, and shows a peculiarity at $T_N$. Fig. 5 shows the imaginary $<\varepsilon_2(\omega)>$ part of the pseudo-dielectric function of $PrFe_3(BO_3)_4$ obtained from the ellipsometry data at different temperatures. Position of the peak in $<\varepsilon_2>$ coincides with the TO frequency, the width is proportional to the damping constant (a negative spike in $<\varepsilon_2(\omega)>$ is, probably, due to diffraction effects at a relatively small crystal area of the $PrFe_3(BO_3)_4$ sample, in the long-wavelength region). Fig. 5 clearly demonstrates a shift and a narrowing of the quasi-phonon mode with lowering the temperature from RT to ~40 K and a progressive loss of its intensity below ~40 K. The quasi-electronic mode gains its intensity from the quasi-phonon mode. A pronounced shift of the quasi-electronic mode to higher frequencies is observed below the temperature of an antiferromagnetic ordering $T_N$ (see Fig. 4 and inset of Fig. 5)

The only difference between the Sm and Pr compounds is that the former has no crystal-field levels below 135 $cm^{-1}$ [17] but the latter possesses a level of $Pr^{3+}$ at ~48 $cm^{-1}$ [19,20], almost resonant with the $A_2^1$ phonon. The symmetry of the corresponding electronic excitation ($\Gamma_2$) coincides with that of the phonon ($A_2$), which favors formation of coupled electron–phonon modes (see, e.g., Refs. [31,32]). Frequencies of the coupled electron–phonon excitations in $PrFe_3(BO_3)_4$ can be found as roots of the following equation [32]:

$$\omega^2 - \omega_0^2 + \frac{2\omega_0\omega_{12}(n_1 - n_2)|W|^2}{\omega^2 - \omega_{12}^2} = 0 \qquad (2)$$

Here $\omega_0$ and $\omega_{12}$ are the frequencies (in $cm^{-1}$) of the vibrational and electronic excitations, respectively, in the absence of interaction; $n_1$ and $n_2$ are relative populations of the excited $|\Gamma_1>$ and ground $|\Gamma_2>$ CF states of $Pr^{3+}$, respectively; $W$ is the interaction constant between the electronic excitation $\omega_{12}$ and the $\Gamma$-point $A_2^1$ optical phonon. This constant determines a change of the RE ion's energy due to a modulation of the crystal field by the $A_2^1$ lattice vibration [32]. At high temperatures, $n_1 \approx n_2$, the electron–phonon interaction vanishes, and we have pure phonon and electronic excitations with frequencies $\omega_+ = \omega_{12}$ and $\omega_- = \omega_0$, respectively. Using Eq. (2), we have modeled the experimental data of Fig. 4. In the case of the Boltzman distribution of populations of electronic levels, the difference of populations $n_1 - n_2$ is given by $n_1 - n_2 = th(\omega_{12}(T)/2kT)$. The function $\omega_{12}(T)$ coincides with the temperature-dependent position of the $Pr^{3+}$ crystal-field level found earlier from optical spectroscopy data [19,20]. The interaction constant $W$ and original phonon frequency $\omega_0$ were varied to achieve the best agreement with the experimental data. This fitting has yielded $\omega_0$=45.5 $cm^{-1}$ and $W$=14.6 $cm^{-1}$.

## 4. Conclusions

Using far-infrared reflection and ellipsometry and Raman scattering spectroscopies, we have performed a study of interactions between the lattice vibrations and the spin system, as well as electronic RE ion crystal-field excitations in multiferroic RE iron borates with the *R*32 structure, $RFe_3(BO_3)_4$, R=Pr, Nd, and Sm. Peculiarities in the temperature dependences of phonon frequencies at the Néel temperature $T_N$ were observed for all the compounds studied. Either hardening or softening below $T_N$ were registered for different modes. The values of the force constants can either grow or diminish in the magnetically ordered state because of (i) atomic displacements due to a local magnetic striction (static mechanism) and (ii) modulation of the exchange interaction by a given vibration (dynamic mechanism). Manifestations of the electron-phonon interaction in $NdFe_3(BO_3)_4$ and a formation of a coupled electron–phonon mode in $PrFe_3(BO_3)_4$ were detected. A rather large value of about 15 $cm^{-1}$ for the electron–phonon coupling constant was found from the modeling

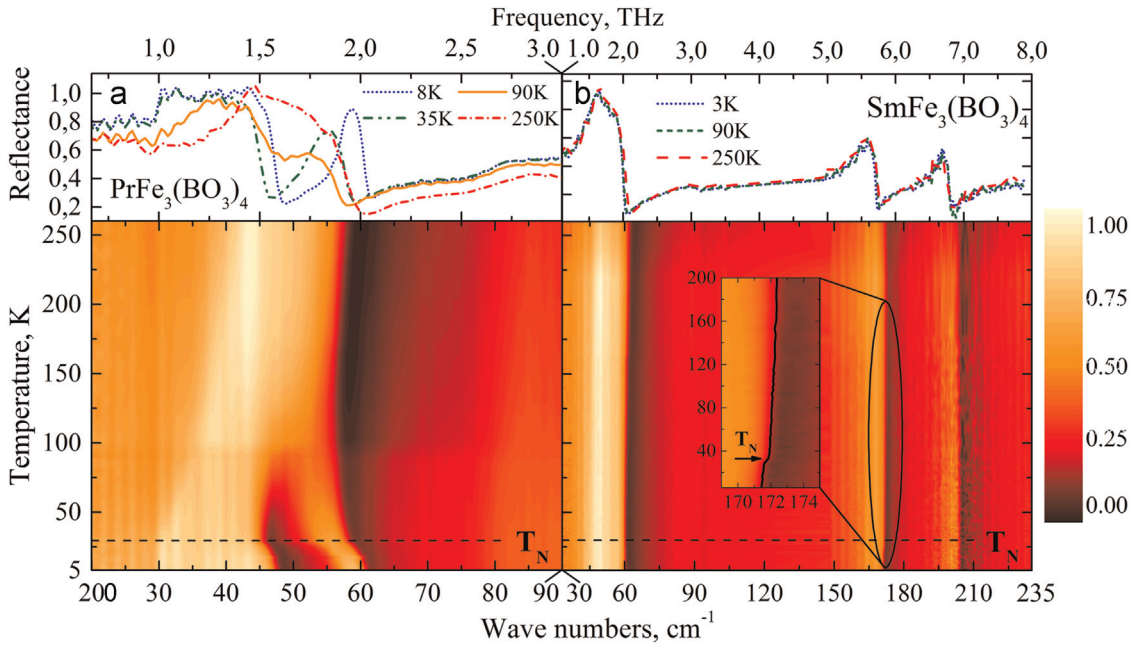


**Fig. 4.** The $\pi$-polarized FIR reflection spectra (upper parts) and the corresponding reflection intensity maps in the frequency-temperature axes (lower parts) for (a) $PrFe_3(BO_3)_4$ and (b) $SmFe_3(BO_3)_4$, $T_N = 32 \pm 1$ K for both compounds. A splitting of the $PrFe_3(BO_3)_4$ reststrahlen band near 50 $cm^{-1}$ below ~100 K is seen. Inset in (b) reveals a small kink at $T_N$ in the $\omega(T)$ dependence for the $A_2^2$ phonon mode of $SmFe_3(BO_3)_4$.

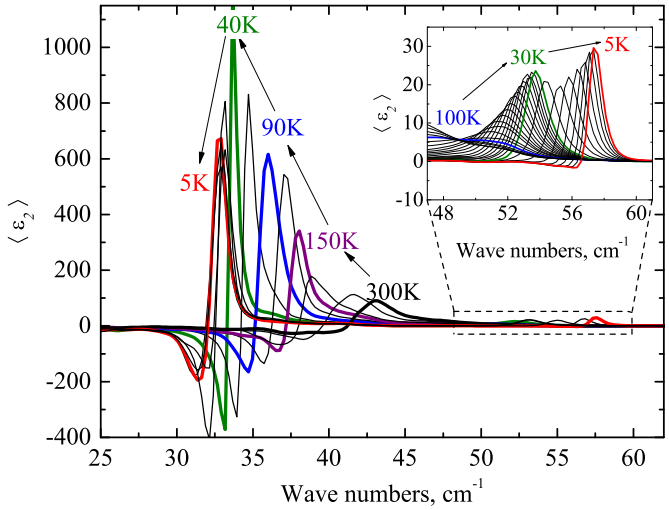


**Fig. 5.** The imaginary $<\varepsilon_2(\omega)>$ part of the pseudo-dielectric function of $PrFe_3(BO_3)_4$ obtained from the ellipsometry data at different temperatures. Inset shows an expanded view of the emerging high-frequency branch of the spectrum.

of a coupled mode behavior in $PrFe_3(BO_3)_4$, which points to an essential role played by the electron–phonon interaction in physics of multiferroics.

## Acknowledgments

This work was supported by the Russian Science Foundation (Grant no. 14-12-01033). Experiments at U4-IR beamline NSLS-BNL (T.N.S. and A.A.S.) were performed under Contract no. DE-FG02-07ER46382 from the U.S. Department of Energy. The National Synchrotron Light Source is operated as a User Facility for the U.S. Department of Energy under Contract no. DE-AC02-98CH10886. M.N.P. thanks B.Z. Malkin for helpful discussions.

## References

[1] S.W. Cheong, M. Mostovoy, Nat. Mater. 6 (2007) 13.
[2] J. van den Brink, D. Khomskii, J. Phys.: Condens. Matter 20 (2008) 434217.
[3] A.P. Pyatakov, A.K. Zvezdin., Phys.–Uspekhi 55 (2012) 557.
[4] R. Haumont, J. Kreisel, P. Bouvier, F. Hippert, Phys. Rev. B 73 (2006) 132101.
[5] V.S. Bhadram, R. Rajeswaran, A. Sundaresan, C. Narayana, EPL 101 (2013) 17008.
[6] K.N. Boldyrev, T.N. Stanislavchuk, S.A. Klimin, M.N. Popova, L.N. Bezmaternykh, Phys. Lett. A 376 (2012) 2562.
[7] T.D. Kang, E. Standard, K.H. Ahn, A.A. Sirenko, G.L. Karr, S. Park, Y.J. Choi, M. Ramazanoglu, V. Kiryukhin, S.W. Cheong, Phys. Rev. B 82 (2010) 014414.
[8] N.I. Leonyuk, L.I. Leonyuk, Progr. Cryst. Growth Charact. 31 (1995) 179.
[9] S.A. Klimin, D. Fausti, A. Meetsma, L.N. Bezmaternykh, P.H.M. van Loosdrecht, T.T.M. Palstra, Acta Crystallogr. B 61 (2005) 481.
[10] D. Fausti, A. Nugroho, P. van Loosdrecht, S.A. Klimin, M.N. Popova, L. N. Bezmaternykh, Phys. Rev. B 74 (2006) 024403.
[11] Y. Hynatsu, Y. Doi, K. Ito, M. Wakeshima, A. Alemi, J. Solid State Chem. 172 (2003) 438.
[12] P. Fisher, V. Pomjakushin, D. Sheptyakov, L. Keller, M. Janoschek, B. Roessli, J. Schefer, G. Petrakovskii, L. Bezmaternikh, V. Temerov, D. Velikanov, J. Phys.: Condens. Matter 18 (2006) 7975.
[13] M. Janoschek, P. Fischer, J. Schefer, B. Roessli, V. Pomjakushin, M. Meven, V. Petricek, G. Petrakovskii, L. Bezmaternikh, Phys. Rev. B 81 (2010) 094429.
[14] J.E. Hamann-Borrero, S. Partzsch, S. Valencia, C. Mazzoli, J. Herrero-Martin, R. Feyerherm, E. Dudzik, C. Hess, A. Vasiliev, L. Bezmaternykh, B. Büchner, J. Geck, Phys. Rev. Lett. 109 (2012) 267202.
[15] E.P. Chukalina, M.N. Popova, L.N. Bezmaternykh, I.A. Gudim, Phys. Lett. A 374 (2010) 1790.
[16] C. Ritter, A. Pankrats, I. Gudim, A. Vorotynov, J. Phys.: Condens. Matter 24 (2012) 386002.
[17] M.N. Popova, E.P. Chukalina, B.Z. Malkin, D.A. Erofeev, L.N. Bezmaternykh and I. A. Gudim, JETP 118, 2014, 111.
[18] A.M. Kadomtseva, Yu F. Popov, G.P. Vorob′ev, A.A. Mukhin, V. Yu., A.M. Ivanov, Kuz′menko, L.N. Bezmaternykh, JETP Lett. 87 (2008) 39.
[19] M.N. Popova, T.N. Stanislavchuk, B.Z. Malkin, L.N. Bezmaternykh, Phys. Rev. Lett. 102 (2009) 187403.
[20] M.N. Popova, T.N. Stanislavchuk, B.Z. Malkin, L.N. Bezmaternykh, Phys. Rev. B 80 (2009) 195101.
[21] C. Ritter, A. Vorotynov, A. Pankrats, G. Petrakovskii, V. Temerov, I. Gudim, R. Szymczak, J. Phys.:Condens. Matter 22 (2010) 206002.
[22] A.K. Zvezdin, G.P. Vorob′ev, A.M. Kadomtseva, Yu F. Popov, A.P. Pyatakov, L. N. Bezmaternykh, A.V. Kuvardin, E.A. Popova, JETP Lett. 83 (2006) 509.
[23] Yu F. Popov, A.P. Pyatakov, A.M. Kadomtseva, G.P. Vorob′ev, A.K. Zvezdin, A. A. Mukhin, V. Yu., Ivanov, I.A. Gudim, JETP 111 (2010) 199.
[24] A.M. Kadomtseva, YuF. Popov, G.N. Vorob′ev, et al., Low Temp. Phys. 36 (2010) 511.
[25] A.A. Mukhin, G.P. Vorob′ev, V. Yu., A.M. Ivanov, A.S. Kadomtseva, A. M. Narizhnaya, Yu F. Kuz′menko, L.N. Popov, Bezmaternykh, I.A. Gudim, JETP Lett. 93 (2011) 275.

[26] T.N. Stanislavchuk, T.D. Kang, P.D. Rogers, E.C. Standard, R. Basistyy, A. M. Kotelyanskii, G. Nita, T. Zhou, G.L. Carr, M. Kotelyanskii, A.A. Sirenko, Rev. Sci. Instrum. 84 (2013) 023901.
[27] K.N. Boldyrev and D.A. Erofeev, Opt. Spectrosc. 116, 2014, 872.
[28] D.J. Lockwood, M.G. Cottam, J. Appl. Phys. 64 (1998) 5876.
[29] A.B. Kuz′menko, D. van der Marel, P.J.M. van Bentum, E.A. Tishchenko, C. Presura, A.A. Bush, Phys. Rev. B 63 (2001) 094303.
[30] M.N. Popova, E.P. Chukalina, T.N. Stanislavchuk, B.Z. Malkin, A.R. Zakirov, E. Antic-Fidancev, E.A. Popova, L.N. Bezmaternykh, V.L. Temerov, Phys. Rev. B 75 (2007) 224435.
[31] J. Kraus, W. Görlitz, M. Hirsch, R. Roth, G. Schaack, Z. Phys. B–Condens. Matter 74 (1989) 247.
[32] A.K. Kupchikov, B.Z. Malkin, A.L. Natadze, and A.I. Ryskin. Spectroscopy of electron–phonon excitations in rare-earth crystals. In Spectroscopy of crystals (in Russian), Nauka, Leningrad, 1989, pp. 84–112.